Continuous wave operation of (Al,In)GaN distributed-feedback laser diodes with high-order notched gratings

Thomas J Slight[1], Szymon Stanczyk[2,3], Scott Watson[4], Amit Yadav[5], Szymon Grzanka[2,3], Edik Rafailov[5], Piotr Perlin [2,3], Stephen P Najda[2], Mike Leszczyński [2,3], Steffan Gwyn[4] and Anthony E Kelly[4]

[1] *Compound Semiconductor Technologies Global Ltd, 6 Stanley Boulevard, G72 0BN, Glasgow, UK*

[2] *Topgan, Sokołowska, 29/37, 01-142 Warsaw, Poland*

[3] *Institute of High Pressure Physics PAS, Prymasa Tysiaclecia 98, 01-424 Warsaw, Poland*

[4] *School of Engineering, University of Glasgow, Glasgow, G12 8LT, UK*

[5]*Aston University, Birmingham, UK, B4 7ET*

E-mail: tslight@compoundsemi.co.uk

We report on the continuous wave, room temperature operation of a distributed-feedback laser diode (DFB-LD) with high-order notched gratings. The design, fabrication and characterization of DFB devices, based on the (Al,In)GaN material system, is described. The uncoated devices were mounted into TO packages for characterization and exhibited single wavelength emission at 408.6 nm with an optical power of 20 mW at 225 mA. A side mode suppression ratio (SMSR) of 35 dB was achieved, with a resolution limited full-width at half maximum of 6.5 pm.

In terms of performance InGaN/GaN DFB-LDs have lagged behind their GaAs and InP counterparts due to a lack of suitable applications to drive development. Of all GaN DFB-LDs reported to date the side mode suppression ration (SMSR) has been low (or not reported) and to the authors knowledge CW operation has only been reported once [1]. For the target applications in this work, in cold-atom based sensing systems [2][3][4], the lasers used must exhibit high SMSR, CW operation, and precise wavelength targeting. Typically, the laser used in these applications is a frequency doubled Ti/Sapphire solid-state laser – replacing these bulky sources with a diode laser would offer many advantages in terms of size reduction and reliability. Other potential applications for these devices are in master oscillator power amplifier systems (MOPA) [5], optical communications systems [6][7][8], medical diagnostics [9] and spectroscopy [10][11].

Single wavelength lasers in the (Al,In)GaN material system have been realised in various ways including use of either buried [12] or surface gratings [13]. Both have their disadvantages, buried gratings require complex overgrowth steps which have the potential to introduce epi-defects and surface grating designs can compromise the quality of the p-type top contact [14] and suffer increased optical losses in electrically un-pumped grating regions. In our approach, gratings are formed along the sidewalls of a ridge waveguide laser diode [15][16][17][18]. It's one of the simplest ways to achieve single wavelength operation and has the advantage that the sidewall grating can be designed and implemented entirely post growth once the emission wavelength is known. Additionally, unlike surface and buried gratings, the coupling coefficient is determined mainly by the planar layout of the grating rather than the etch depth, therefore increasing design freedom.

The principal of operation for this device is similar to that described in [19][20], where in essence a Fabry-Perot (FP) laser is provided with weak optical feedback by a high order grating that runs along the partial length of the waveguide. High order DFB designs have been demonstrated to have intrinsically narrower linewidths than conventional DFB laser diodes [21] and so could be particularly suited to spectroscopic applications. The feedback from the high order grating is sufficient to allow lasing in a single or narrow band of FP modes which are close in wavelength to the Bragg wavelength (λ_B), with FP modes away from λ_B experiencing an increased optical loss penalty. In order to ensure single wavelength operation, the grating must have a reflection bandwidth that is on the same order as the free

spectral range (FSR) of the cavity (<0.1nm). There are some significant differences in how we have implemented this concept in a GaN laser compared to the equivalent device in InP or GaAs. Firstly, the index perturbations are achieved using a sidewall grating rather than a surface grating. This maximizes the surface area of the p-contact in order to minimise resistance (ohmic contacts to P-GaN tend to have a relatively high specific contact resistance [22]). Also, since the entire top surface of the waveguide is electrically contacted, we avoid large optical losses in un-pumped regions (potentially as high 15 to 30 cm^{-1} due to the p doped cladding & contact layers [23]).

The second challenge in implementing the high order grating design is that the free spectral range, (given by $\Delta\lambda_{FSR} = \lambda^2/2n_{eff,g}L_{cav}$ where λ is the emission wavelength, L_{cav} is the cavity length, & $n_{g,eff}$ is the effective group index) of the Fabry-Perot cavity in a GaN laser is an order of magnitude smaller than for an InP based laser (e.g. for a 1000 μm long resonator the FSR is 0.03 nm at 420 nm vs 0.4nm at 1550 nm) hence the reflection bandwidth of the grating must be much narrower for GaN. The grating bandwidth is dependent on the reflectivity of each notch pair; the lower the reflectivity per notch pair the narrower the bandwidth, but a larger number of pairs are required to maintain the required total reflectivity. We used the TMM (transmission matrix method [24]) to estimate the number of notch pairs required. Effective modal indices were calculated using a 2D optical mode solver for both perturbed (notched) and unperturbed sections of the waveguide. The indices were then used along with a TMM solver to calculate the reflection bandwidth of the grating. This technique is approximate [25] but gives us an estimate of the required quantity of notches to achieve single wavelength operation. Our design used a 39th order grating with 125 notch pairs along the ridge which we estimate to have a bandwidth ~0.1 nm (fig 1a).

In addition to the closely spaced FP cavity resonances there are more widely spaced resonances corresponding to the different orders of Bragg reflection from the grating. Increasing the wavelength range with the TMM model we can see that there are additional reflectivity peaks at ~398 nm & ~419 nm due to 38^{th} and 40^{th} order Bragg reflections respectively (fig. 1b). As a consequence, it is important that we design the grating such that the FSR is wider than the gain spectrum of the laser to ensure single wavelength operation and to minimize the chances of mode hopping between grating resonances.

Devices were fabricated from AlInGaN laser epi-structures, consisted of three InGaN

quantum wells sandwiched between GaN barriers, GaN waveguide layers and $Al_{0.06}Ga_{0.94}N$ cladding layers. The quantum wells thicknesses were designed for emission at around 410 nm. The ridge/grating pattern was defined by electron beam lithography (Raith VB6 electron beam lithography system with a write resolution of 1 nm) – see fig 2. The pattern was first written into ZEP 520 resist which was then transferred into a 120 nm thick layer of SiO_2 using reactive ion etching (RIE). The ZEP resist was then removed to leave the SiO_2 as a mask suitable for Inductively coupled plasma (ICP) etching. An optimized ICP process with a Cl_2/N_2 chemistry [26] [27] gave a smooth and vertical etch profile, important in achieving optimal grating performance. The as etched waveguide is shown if fig. 2. Once etched, a layer of SiO_2 was deposited to act as an insulator between the metal contact pads and the semiconductor. Via's were etched in this layer to contact the top of the waveguide ridge and a layer of Ni/Au was deposited by evaporation to act as an ohmic contact [28] with a further layer of Ti/Pt/Au deposited to enable wire bonding. The sample was then thinned/polished, back metal deposited, and then cleaved into individual chips. The uncoated chips were then mounted into TO 5.6 mm cans for testing.

The samples were placed on a thermoelectric cooler (TEC) and stabilized to 20℃. The temperature was measured by thermocouple placed inside copper holder, near the position of the TO 5.6 can. The temperature was stabilized to 20^{o}C by TEC controller. The laser diodes were driven by laser diode controller (Thorlabs ITC4005QCL) in CW operation. The light emitted by the devices was collimated by an aspheric plano-convex lens with low focal length and large numerical aperture (NA = 0.55). The optical power was measured to a standard photodiode power sensor connected to a power meter (Thorlabs S121C and PM320E). The emission spectra were acquired using a high-resolution 1 m long spectrometer (FHR1000 Horiba Jobin Yvon equipped with a Synapse 2048 x 512 CCD camera and a 3600 groove per mm diffraction grating) with a resolution of approximately 6.5 pm.

Fig 3 shows the voltage and optical power as a function of drive current for a 39th order grating DFB LD with 1.5 μm / 2.5 μm grating widths, a cavity length of 1000 μm and an etch depth of 520 nm. The measured threshold current is 130 mA and the slope efficiency is 0.27 W/A (for an uncoated device). The optical power characteristic displayed a kink at 160 mA which is thought to be due to mode hops between adjacent FP modes caused by

differences in the shift of gain curve and RI with temperature. Fig 4. shows the emission spectrum measured at a drive current of 225 mA (1.73* Ith), the SMSR is 35 dB at a CW optical output power of 20 mW. The emission spectrum for different driving currents is shown in fig. 5, with Fabry-Perot resonances apparent below threshold and a switch to single wavelength emission above, red-shifting with increased current and hence temperature. The quantitative dependence of wavelength on temperature was not measured due to the difficulty of determining the CW chip temperature but for a similar device by the authors, operated under pulsed conditions, the tuning coefficient was 0.012 nm/K [16].

The notched lasers showed both two times higher threshold current and two times lower efficiency than Fabry-Perot lasers processed from the same wafer. The comparison of the LI characteristics for FP-LD and DFB-LD is shown in Fig 6 and the comparison of the spectrum for I = 150 mA is shown in Fig. 7.

We believe the compromised performance of the DFB-LD over the FP-LD is due to optical losses occurring in the notched section of the waveguide. It is shown in [25] using the scattering matrix method (SMM) that light is scattered as it transits from unperturbed to perturbed (notched) regions. By minimizing the number notch pairs while maintaining the bandwidth necessary for single wavelength operation it should be possible to improve performance. The application of HR/AR optical coatings to the laser facets should also reduce threshold current and increase slope efficiency [29][30].

We have demonstrated (Al,In)GaN distributed feedback laser diodes utilizing 39^{th} order gratings exhibiting CW single mode output powers of 20 mW with a SMSR better than 35 dB. The design offers a simplified fabrication route without regrowth and with more easily achievable feature sizes over lower order gratings. To further improve performance, optimised grating designs and anti-reflective facet coatings could be used in order to increase power and decrease threshold current. Single-frequency GaN laser devices of this type will find applications in laser cooling and communications.

Acknowledgments

This research has been supported by the European Union with grant E10509, Innovate UK through grant 132543, and by the National Centre for Research and Development with grants E10509/29/NCBiR/2017 and 1/POLBER-3/2018).

References

1) S. Masui, K. Tsukayama, T. Yanamoto, T. Kozaki, S.I. Nagahama, and T. Mukai, Japanese J. Appl. Physics, Part 2 Lett. 45, 1223 (2006).
2) Y. Shimada, Y. Chida, N. Ohtsubo, T. Aoki, M. Takeuchi, T. Kuga, and Y. Torii, Rev. Sci. Instrum. 84, (2013).
3) P. Dubé, A.A. Madej, J.E. Bernard, and A.D. Shiner, in (2007), pp. 667305–667312.
4) A. Shiner, Development of a Frequency Stabilized 422-Nm Diode-Laser System and Its Application to A 88Sr+ Single Ion Optical Frequency Standard (York University, 2006).
5) 1 S. Stanczyk, A. Kafar, S. Grzanka, M. Sarzynski, R. Mroczynski, S. Najda, T. Suski, and P. Perlin, Opt. Express 26, 7351 (2018).
6) Y.-C. Chi, D.-H. Hsieh, C.-T. Tsai, H.-Y. Chen, H.-C. Kuo, and G.-R. Lin, Opt. Express 23, 13051 (2015).
7) T.-C. Wu, Y.-C. Chi, H.-Y. Wang, C.-T. Tsai, and G.-R. Lin, Sci. Rep. 7, 40480 (2017).
8) S. Watson, M. Tan, S.P. Najda, P. Perlin, M. Leszczynski, G. Targowski, S. Grzanka, and a E. Kelly, Opt. Lett. (2013).
9) S.P. Najda, P. Perlin, M. Leszczynski, T.J. Slight, W. Meredith, M. Schemmann, H. Moseley, J.A. Woods, R. Valentine, S. Kalra, P. Mossey, E. Theaker, M. MacLuskey, G. Mimnagh, and W. Mimnagh, in Prog. Biomed. Opt. Imaging - Proc. SPIE (2015).
10) H. Leinen, D. Gläßner, H. Metcalf, R. Wynands, D. Haubrich, and D. Meschede, Appl. Phys. B Lasers Opt. 70, 567 (2000).
11) B. Li, S. Luo, A. Yu, J. Gao, P. Sun, X. Wang, and D. Zuo, Laser Phys. Lett. (2017).
12) D. Hofstetter, R.L. Thornton, L.T. Romano, D.P. Bour, M. Kneissl, and R.M. Donaldson, Appl. Phys. Lett. 73, 2158 (1998).
13) D. Cortaberria and S. Yu, in Quantum Electron. Laser Sci. Conf. (2005), pp. 1023–1025.
14) S.J. Pearton, J.W. Lee, J.D. MacKenzie, C.R. Abernathy, and R.J. Shul, Appl. Phys. Lett. 67, 2329 (1995).

15) T.J. Slight, O. Odedina, W. Meredith, K.E. Docherty, and A.E. Kelly, IEEE Photonics Technol. Lett. 28, 2886 (2016).
16) T.J. Slight, A. Yadav, O. Odedina, W. Meredith, K.E. Docherty, E. Rafailov, and A.E. Kelly, IEEE Photonics Technol. Lett. 29, 2020 (2017).
17) J.H. Kang, H. Wenzel, V. Hoffmann, E. Freier, L. Sulmoni, R. Unger, S. Einfeldt, T. Wernicke, and M. Kneissl, IEEE Photonics Technol. Lett. 30, 231 (2018).
18) H. Schweizer, H. Gräbeldinger, V. Dumitru, M. Jetter, S. Bader, G. Brüderl, A. Weimar, A. Lell, and V. Härle, Phys. Status Solidi Appl. Res. 192, 301 (2002).
19) R. Phelan, W.H. Guo, Q. Lu, D. Byrne, B. Roycroft, P. Lambkin, B. Corbett, F. Smyth, L.P. Barry, B. Kelly, J. O'Gorman, and J.F. Donegan, IEEE J. Quantum Electron. 44, 331 (2008).
20) Q. Lu, W.H. Guo, D. Byrne, and J.F. Donegan, IEEE Photonics Technol. Lett. 22, 787 (2010).
21) Y. Wang, Y. Yang, S. Zhang, L. Wang, and J.J. He, IEEE Photonics Technol. Lett. 24, 1233 (2012).
22) J.O. Song, J.S. Ha, and T.Y. Seong, IEEE Trans. Electron Devices 57, 42 (2010).
23) E. Kioupakis, P. Rinke, and C.G. Van De Walle, Appl. Phys. Express 3, 82101 (2010).
24) M. Born, E. Wolf, A.B. Bhatia, P.C. Clemmow, D. Gabor, A.R. Stokes, A.M. Taylor, P.A. Wayman, and W.L. Wilcock, Principles of Optics, 7th ed. (Cambridge University Press, 1999).
25) Q.Y. Lu, W.H. Guo, R. Phelan, D. Byrne, J.F. Donegan, P. Lambkin, and B. Corbett, IEEE Photonics Technol. Lett. 18, 2605 (2006).
26) S.J. Pearton, R.J. Shul, and F. Ren, MRS Internet J. Nitride Semicond. Res. 5, (2000).
27) R.J. Shul, G.B. McClellan, S.A. Casalnuovo, D.J. Rieger, S.J. Pearton, C. Constantine, C. Barratt, R.F. Karlicek, C. Tran, and M. Schurman, Appl. Phys. Lett. 69, 1119 (1996).
28) J.K. Ho, C.S. Jong, C.C. Chiu, C.N. Huang, K.K. Shih, L.C. Chen, F.R. Chen, and J.J. Kai, J. Appl. Phys. 86, 4491 (1999).
29) M.X. Feng, S.M. Zhang, D.S. Jiang, H. Wang, J.P. Liu, C. Zeng, Z.C. Li, H.B. Wang, F. Wang, and H. Yang, Sci. China Technol. Sci. (2012).
30) R.M. Farrell, P.S. Hsu, D.A. Haeger, K. Fujito, S.P. Denbaars, J.S. Speck, and S. Nakamura, Appl. Phys. Lett. 96, (2010).

Figure Captions

Fig. 1. a) Reflectance spectrum modeled using TMM method with FWHM of 0.11 nm. b) The spectrum over a larger scale to show additional grating resonances

Fig. 2. SEM micrograph of the as etched ridge with 39th order side wall grating.

Fig. 3. Optical power and voltage as a function of DC drive current.

Fig. 4. Emission spectra at drive current of 225 mA on dB scale over small wavelength range. The SMSR is greater than 35 dB.

Fig. 5. Emission spectra for a range of drive currents.

Fig. 6. The comparison of the LI characteristics between a standard FP laser diode and for the DFB laser diode

Fig. 7. Comparison of the spectrum between the standard LD and FP laser diode for driving current I = 150 mA.

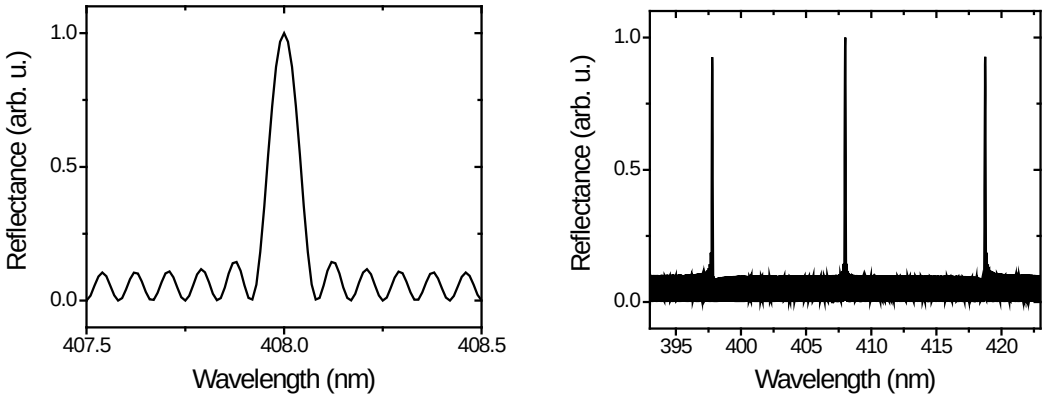
Reflectance (arb. u.)
1.0
0.5
0.0
407.5
408.0
408.5
Wavelength (nm)
Reflectance (arb. u.)
1.0
0.5
0.0
395
400
405
410
415
420
Wavelength (nm)

(a) (b)

Fig. 1.

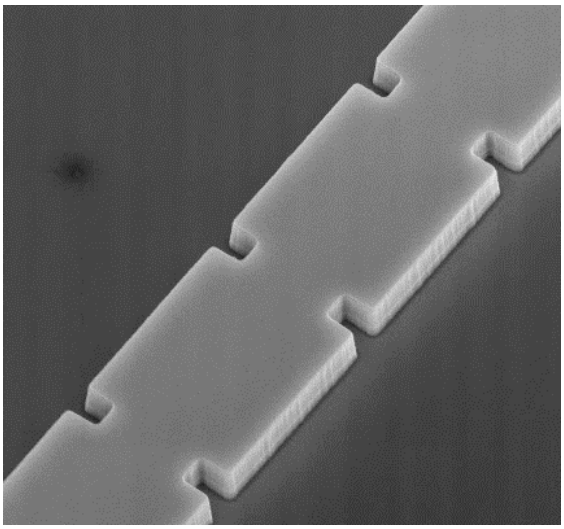

Fig. 2.

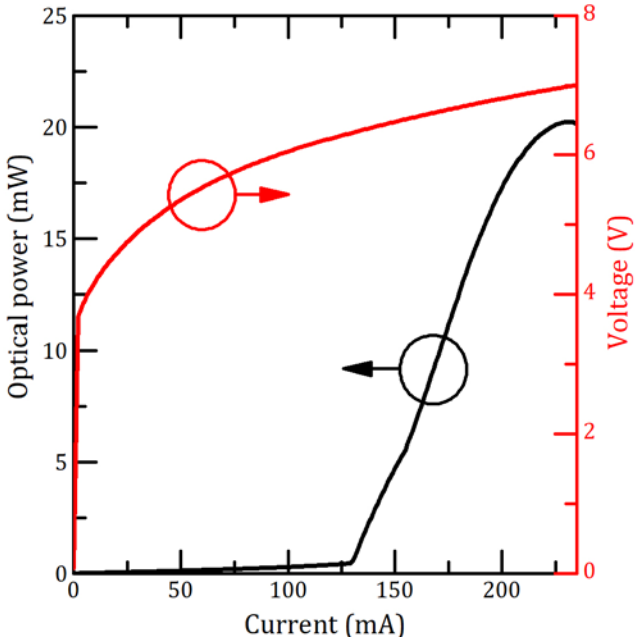
Optical power (mW)
Voltage (V)
Current (mA)
0
5
10
15
20
25
0
2
4
6
8
0
50
100
150
200

Fig. 3.

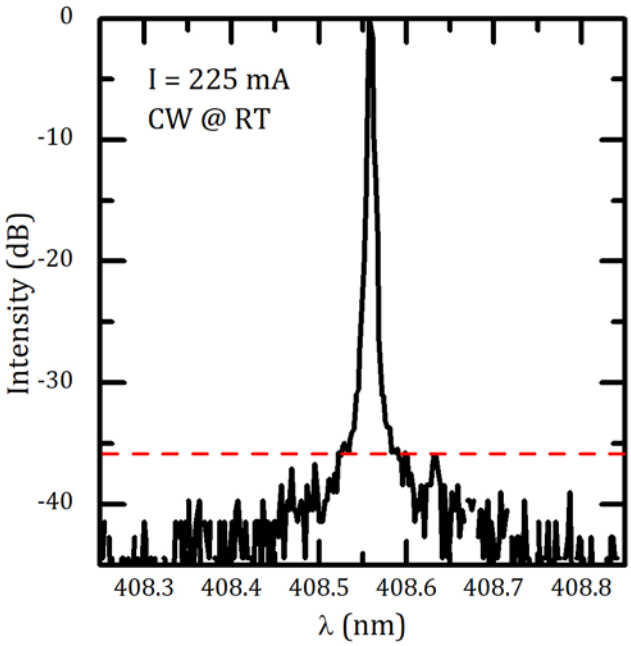
I = 225 mA
CW @ RT
Intensity (dB)
λ (nm)
0
-10
-20
-30
-40
408.3
408.4
408.5
408.6
408.7
408.8

Fig. 4.

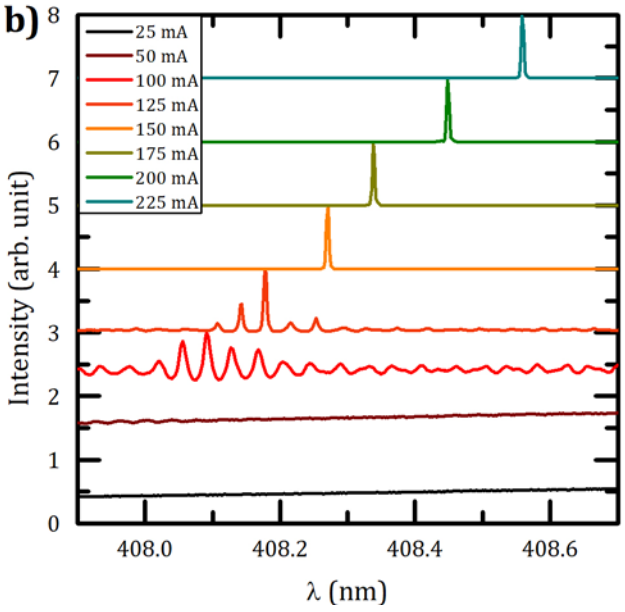
b)
25 mA
50 mA
100 mA
125 mA
150 mA
175 mA
200 mA
225 mA
Intensity (arb. unit)
λ (nm)
0
1
2
3
4
5
6
7
8
408.0
408.2
408.4
408.6

Fig. 5.

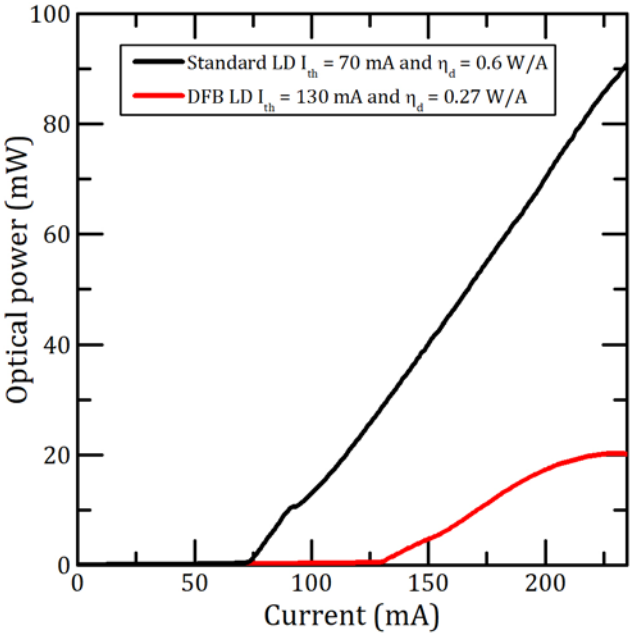
Standard LD I_th = 70 mA and η_d = 0.6 W/A
DFB LD I_th = 130 mA and η_d = 0.27 W/A
Optical power (mW)
Current (mA)
0
20
40
60
80
100
0
50
100
150
200

Fig. 6.

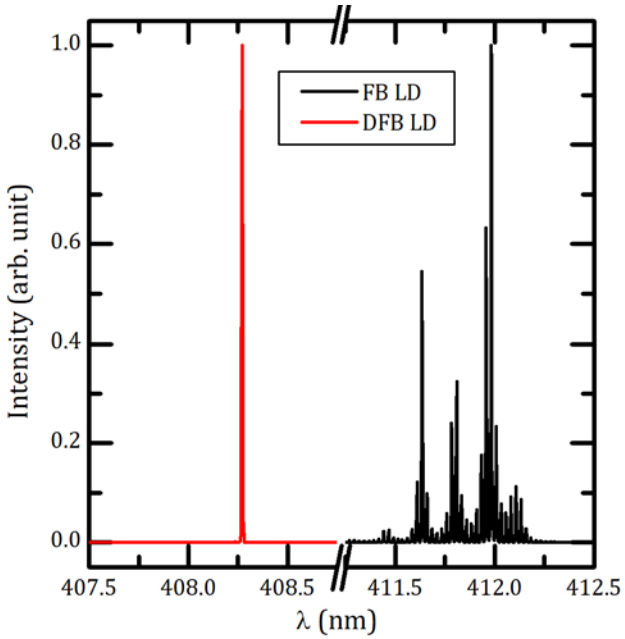
FB LD
DFB LD
Intensity (arb. unit)
1.0
0.8
0.6
0.4
0.2
0.0
407.5
408.0
408.5
411.5
412.0
412.5
λ (nm)

Fig. 7.